Phys. Med. Biol. **54** (2009) N29–N35 doi:10.1088/0031-9155/54/2/N01

NOTE

Comparison of two dedicated 'in beam' PET systems via simultaneous imaging of ^{12}C-induced β^+-activity

F Attanasi[1], N Belcari[1], A Del Guerra[1], W Enghardt[2,3], S Moehrs[1], K Parodi[4], V Rosso[1] and S Vecchio[1]

[1] Università di Pisa and Istituto Nazionale di Fisica Nucleare (INFN), Largo B. Pontecorvo 3, 56127 Pisa, Italy
[2] Forschungszentrum Rossendorf, Institute of Nuclear and Hadron Physics, PO Box 510119, 01314 Dresden, Germany
[3] Technische Universität Dresden, Radiation Research in Oncology-Oncoray, Fetscherstr. 74, PO Box 86, 01307 Dresden, Germany
[4] Heidelberg Ion Beam Therapy Center (HIT), Im Neuenheimer Feld 450, 69120 Heidelberg, Germany

E-mail: sara.vecchio@pi.infn.it

Received 8 August 2008, in final form 21 October 2008
Published 16 December 2008
Online at stacks.iop.org/PMB/54/N29

Abstract
The selective energy deposition of hadrontherapy has led to a growing interest in quality assurance techniques such as 'in-beam' PET. Due to the current lack of commercial solutions, dedicated detectors need to be developed. In this paper, we compare the performances of two different 'in-beam' PET systems which were simultaneously operated during and after low energy carbon ion irradiation of PMMA phantoms at GSI Darmstadt. The results highlight advantages and drawbacks of a novel in-beam PET prototype against a long-term clinically operated tomograph for ion therapy monitoring.

(Some figures in this article are in colour only in the electronic version)

1. Introduction

Hadrontherapy benefits from a more selective energy deposition in depth with respect to conventional radiotherapy. The superior dose conformality offered by this modality demands a higher accuracy in the planning and delivery of the treatment. This has led to a growing interest in quality assurance techniques such as 'in-beam' (i.e., during the irradiation) positron-emission-tomography (PET). The feasibility and clinical value of in-beam PET has already been demonstrated for ^{12}C ion therapy using a dedicated, double-head PET scanner completely integrated into the treatment room of the experimental therapy unit at the Gesellschaft für Schwerionenforschung (GSI) Darmstadt (Enghardt *et al* 1999a, 1999b, 2004, Parodi 2004).

The method used at GSI to verify particle beam dose delivery is to simulate the expected PET activation and compare it with the actual measurement (Pönisch *et al* 2004). Motivated by this clinical experience and in connection with the rapidly growing number of ion beam therapy facilities worldwide, an increasing interest has been devoted to PET imaging for quality assurance not only of carbon ions but also of protons (Litzenberg *et al* 1999, Parodi *et al* 2002, Inaniwa *et al* 2005), ^{3}He (Fiedler *et al* 2006), ^{16}O (Inaniwa *et al* 2008) and even photons (Möckel *et al* 2007). Besides the already clinically operated in-beam PET tomograph at GSI or the post-irradiation ('offline') usage of commercial full-ring PET or PET/CT scanners (Hishikawa *et al* 2002, Parodi *et al* 2007), new experimental planar positron cameras suited for in-beam installation have been recently realized at HIMAC (Iseki *et al* 2003), Kashiwa (Nishio *et al* 2006) and Pisa (Attanasi *et al* 2008a). This paper focuses on the latter system, that was developed inside the DoPET project (dosimetry with a positron emission tomograph). The validation of this small system was performed at the INFN Laboratori Nazionali del Sud (LNS) by using 62 MeV protons stopped in PMMA phantoms (Vecchio *et al* 2007, Attanasi *et al* 2008b). In perspective of the foreseen application of the DoPET prototype for all the relevant ion beam modalities, it is important to validate the performances of the system for the increasingly considered carbon ion case. In a first experiment performed at GSI, the performances of the DoPET prototype were investigated against those of the clinically established BASTEI detector (beta activity measurements at the therapy with energetic ions, Enghardt *et al* 2004a, Crespo *et al* 2006) for simultaneous imaging of PMMA ($C_5H_8O_2$) activation induced by low energy ^{12}C-ion beams, as reported in the following.

2. Materials and methods

2.1. PET imaging systems

2.1.1. BASTEI detector. It consists of two detector heads with 42 × 21 cm^2 front area each, based on bismuth germanate (BGO) square crystals (6.75 mm pitch) coupled to PMT. The total detection efficiency at the center of the positron camera is approximately 2.3% in the fixed energy window [250, 850] keV (Fiedler *et al* 2006). The energy resolution is about 16% at 511 keV, the spatial resolution varies between 5 and 7 mm (FWHM) in the central plane parallel to detector heads. Synchronization of in-beam PET imaging with the time structure of the pulsed beam delivery allows data acquisition to be performed during the irradiation. This modality allows one to benefit from the decays in the pauses of the beam delivery when the γ-ray background produced by beam-induced nuclear reactions is low. A backprojection reconstruction algorithm is adopted for data analysis of small treatment volumes in the center of the field of view (Parodi *et al* 2005). The algorithm includes corrections for random events, attenuation and spatially varying detection efficiency.

2.1.2. DoPET detector. The imaging prototype consists of two planar detector heads, offering an active area of about 4.5 × 4.5 cm^2. One head is made up of 21× 21 lutetium–yttrium oxyorthosilicate (LYSO) square crystals (2 mm size, 2.15 mm pitch) coupled to one squared multi-anode PMT (Hamamatsu H8500), offering an active area of 49 × 49 mm^2 (Vecchio *et al* 2007). The movable detector heads have been placed symmetrically with respect to the measured activity region, diametrically opposed and 14 cm apart. The energy resolution is less than 16% at 511 keV and the detection efficiency measured at the center of the field of view (FoV) was about 0.7% in the energy window [350, 850] keV usually adopted to reject the natural crystal radioactivity. The activity distributions are reconstructed using a 3D maximum likelihood expectation maximization (ML-EM) algorithm, using a probability matrix based

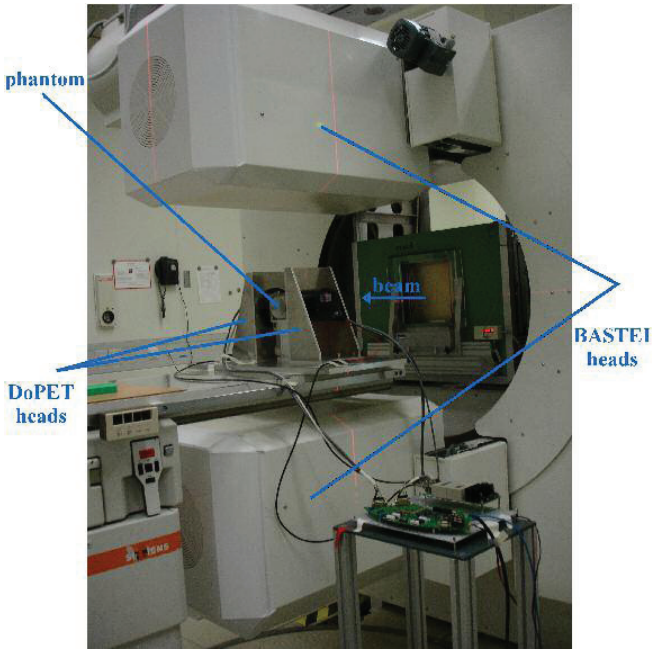

Figure 1. Experimental configuration for comparison of the PET systems, marked by the corresponding lines and text in the image. As a common reference system, z is the vertical direction ($z = 0$ at the isocenter) and x is the beam direction ($x = 0$ at the phantom entrance surface).

on a multi-ray approach and allowing corrections for random coincidences as well as for non-uniform detection efficiency (Moehrs *et al* 2008). The reconstructed dimension of a ^{22}Na point source along the beam direction results in 1.7 mm (FWHM). At present there is no possibility of synchronizing the data acquisition with an external signal from a pulsed beam delivery.

2.2. Irradiation setup

Measurements were performed using ^{12}C ion beams in the energy range below 117 MeV u^{-1} from the GSI synchrotron in Darmstadt. The maximum beam energy was chosen so that the entire ion path was contained within the smallest FoV of the two PET cameras. Irradiations were delivered to cylindrical PMMA phantoms of 7 cm diameter and 7 cm length. The cylinder base was oriented orthogonally to the impinging beam.

The two PET devices were placed as shown in figure 1. The centers of the fields of view have been aligned to the isocenter of the treatment room, with the help of the two orthogonal lasers. Once the detectors were aligned for carbon beam delivery, a ^{22}Na point source was placed in front of the phantom entrance surface, and acquired with the BASTEI scanner as a further check of the system reference. Appropriate attenuation correction was introduced in image reconstruction of BASTEI data, in order to take into account the presence of the aluminum mechanical system of the DoPET detector in the field of view of the BASTEI detector.

Three monoenergetic configurations were used for scanned carbon irradiations: 108.53 MeV u^{-1}, 112.60 MeV u^{-1} and 116.57 MeV u^{-1}. The carbon ion ranges in water

for the chosen energies are derived from the treatment planning system TRiP98 (Krämer *et al* 2000) and converted in PMMA range using a measured scaling factor of 1.165 (Jäkel *et al* 2001). The resulting range values in PMMA are 22.2 mm, 23.9 mm and 25.6 mm, respectively. A weighted combination of the three energies was also used for a spread-out Bragg peak (SOBP) irradiation, 3.4 mm width at 95% level. In all cases, a squared transversal section of 28 mm side was adopted. The delivered dose was 60 Gy for each treatment field, divided as six beam repainting of 10 Gy each. The irradiation delivered by the GSI synchrotron is pulsed. Beam extraction (spill) at a selected energy, focus and intensity has a period of about 5 s, with a maximum spill duration of about 2 s. The remaining time before the next spill (spill pause) is required for beam injection and acceleration. A complete beam delivery consists in repetitions of several spills and pauses. The total time required for monoenergetic irradiation spanned from 2 to 3 min. The spread-out irradiation lasted about 6 min.

2.3. Data acquisition and reconstruction

The acquisitions of the two PET systems were performed simultaneously. They were started manually at the beginning of the irradiation, and lasted about 31 min each. Off-line selection of time interval for data analysis was performed. Data belonging to the first 3 min for monoenergetic irradiation and 6 min for SOBP were discarded in the analysis of DoPET acquisitions, since no beam on/off tagging was available for the rejection of the high γ background during spills. About 2×10^5 events were then available after each irradiation for an effective acquisition time of 28 min (monoenergetic) and 25 min (SOBP). For the BASTEI acquisition, more than 3×10^4 events collected in the spill pauses could be analyzed together with the $1.5–1.7 \times 10^5$ events decayed in the 28 min following the end of irradiation. About 2×10^5 events were then collected, as expected from the detection efficiency combined with the attenuation effect produced by DoPET mechanical support. Reconstructed images had a dimension of $42 \times 42 \times 42$ voxels (1.076 mm in size) for DoPET, and $60 \times 60 \times 60$ voxels of 1.6875 mm size for BASTEI.

3. Results and discussion

Longitudinal profiles and contour plots in the planes parallel to the detector heads were calculated from reconstructed activities and are displayed in figures 2 and 3. The xz and xy planes are adopted for DoPET and BASTEI detectors, respectively. The carbon beam impinges from the left. The central image profiles along beam direction x for the two systems were produced by averaging all the longitudinal profiles on a 25 mm $\times$ 25 mm irradiated area. This is equivalent to 23×23 DoPET voxels and 15×15 BASTEI voxels. Integration over 25 mm along the axis with the worst spatial resolution (y for DoPET images, and z for BASTEI) was done for the contour plot representation of the activity. Due to the symmetry under 90° rotation of the squared irradiation field, a comparison of such contour plots can be done.

Both detectors reconstruct activity distributions that allow a good separation of the Bragg peaks. As a parameter to appreciate the spatial separation of ^{11}C activity profiles we chose the distance between the activity peaks starting from the deepest. The shift measured between 112.60 MeV u^{-1} and 116.57 MeV u^{-1} irradiations are 1.8 mm for BASTEI and 1.7 mm for DoPET, respectively. The shift measured between 108.53 MeV u^{-1} and 116.57 MeV u^{-1} irradiations is 3.8 mm for both detectors. The FWHM of the activation peak is about 14 mm for BASTEI and about 6 mm for DoPET, for all three irradiations.

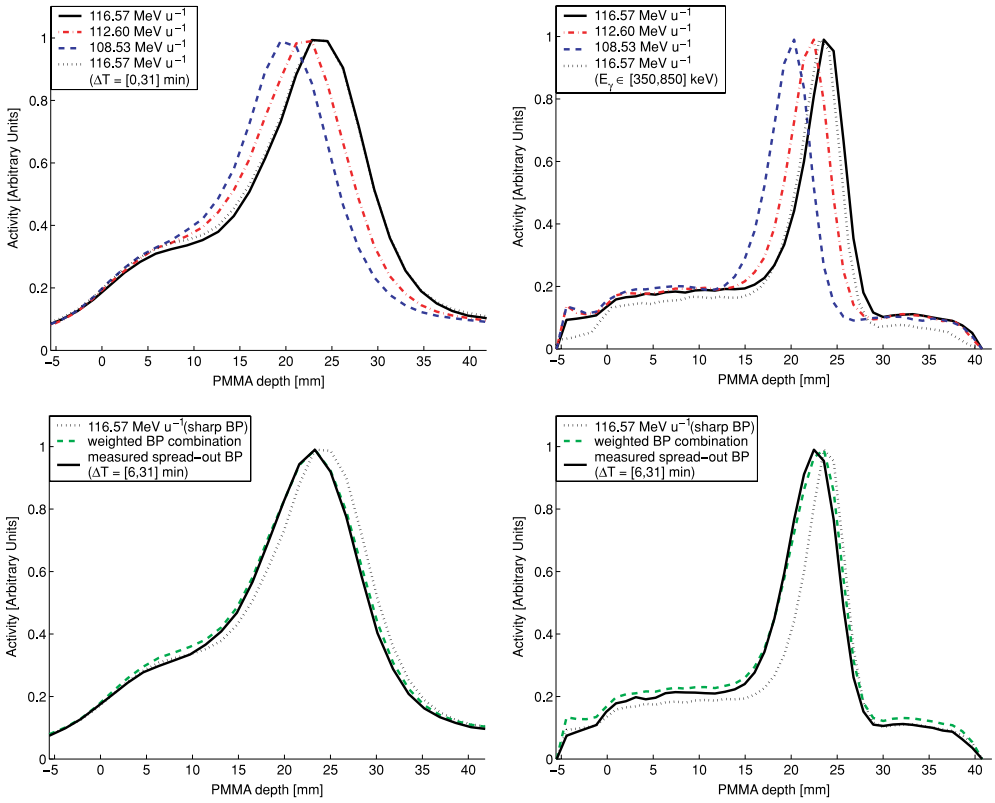

Figure 2. Transversally integrated longitudinal profiles from reconstructed image of activity acquired by BASTEI left and DoPET right systems during and after ^{12}C irradiations. Where not specified in the legend, energy selection is [250, 850] keV and acquisition time interval is [3, 31] min.

Reconstruction of the BASTEI data including the first 3 min after beginning of irradiation is shown as the dotted line in the figure 2(a). A very small reduction of the peak-to-plateau ratio is observed. Since the BASTEI detector starts to acquire β^+ decays in the spill pauses during carbon irradiation, the acquired activity contains a significant contribution from short-lived emitters like ^{15}O, which derives from target activation, and can be seen only in the activity plateau before the Bragg peak. The change in spatial pattern of activation related to the acquisition start, i.e. to the ratio of ^{15}O and ^{11}C decays detected, has already been shown (Pönisch *et al* 2004). From the reconstruction of the DoPET data in a more selective energy window (dotted line in figure 2(b)), one can appreciate the increased rejection of background from the LYSO intrinsic radioactivity and from scattered radiation, resulting in a better definition of the activity profiles at the phantom edge (0 mm) and of the target-to-projectile activation ratio.

As results from figures 2(a) and (b), both tomographs are able to detect the 1.8 mm ^{12}C range shifts expected from the beam energy increase. Figures 2(c) and (d) show how the difference between sharp and spread-out Bragg peak is detected by the two systems. As a reliability check, the activity measured from the spread-out irradiation is compared with a weighted combination of the activities measured from the three monoenergetic

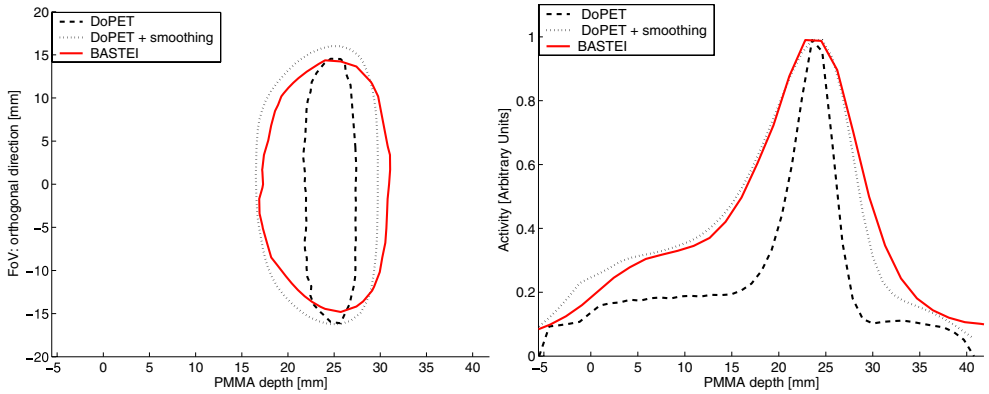

Figure 3. Comparison of reconstructed image of activity acquired by DoPET and BASTEI systems after ^{12}C irradiations, using the energy selection [250, 850] keV. Left: 50% contour plots in the xy and xz planes. Right: average profiles along x.

irradiations. The weights for the linear combination of reconstructed images are derived from those of three peaks in the spread-out irradiation: 0.595, 0.210 and 0.195 for 108.53 MeV u^{-1}, 112.60 MeV u^{-1} and 116.57 MeV u^{-1}, respectively.

In figure 3 the activity distributions reconstructed using the same time and energy selections are compared for the two systems. Differences are mainly due to the spatial resolution as well as to the angular coverage and to the reconstruction algorithm. As a validation, data produced after a 13 mm (FWHM) Gaussian smoothing on DoPET image is also shown.

4. Conclusion and outlook

In the small field of view, the performances of the novel DoPET prototype are similar to those of the clinically established BASTEI tomograph in terms of range resolvability, while exhibiting a superior spatial resolution due to the smaller crystal. This supports its applicability to monitor treatment of small lesions in the case of carbon ion therapy. However, the limited geometrical detection efficiency as well as the required rejection of decay events from the first minutes penalized the counting statistics and the ^{15}O fraction of the simultaneously imaged activation. Both these drawbacks can be overcome by an upgraded system with an enlarged detection area and the availability of an external trigger signal in the acquisition system so as to tag the acquired data for real in-beam operation. A system that fulfils these requirements is included in a proposed research project for the development of an innovative treatment planning system for hadrontherapy by several INFN groups (Agodi *et al* 2008).

Acknowledgments

We are grateful to all those people who made the data acquisition at GSI possible. Among them we thank T Haberer (HIT) for organizing the beam time, D Schardt (GSI) and S Brons (HIT) for support in preparation of the experiment.

References

Attanasi F *et al* 2008a Preliminary results of an in-beam PET prototype for proton therapy *Nucl. Instrum. Methods* A **591** 296–9

Attanasi F *et al* 2008b Experimental validation of the filtering approach for dose monitoring in proton therapy at low energy *Phys. Med.* **24** 102–6

Agodi C *et al* 2008 The INFN TPS project *Nuovo Cimento* C **31** 99–108

Crespo P A V, Shakirin G and Enghardt W 2006 On the detector arrangement for in-beam PET for hadron therapy monitoring *Phys. Med. Biol.* **51** 2143–63

Enghardt W *et al* 1999a The routine PET monitoring of tumour therapy with ^{12}C ions *Forschungszentrum Rossendorf Annual Report* FZR-271 89–90

Enghardt W, Debus J, Haberer T, Hasch B G, Hinz R, Jäkel O, Krämer M, Lauckner K, Pawelke K and Pönisch F 1999b Positron emission tomography for quality assurance of cancer therapy with light ion beams *Nucl. Phys.* A **654** 1047c–50c

Enghardt W, Crespo P, Fiedler F, Hinz R, Parodi K, Pawelke J and Pönisch F 2004 Charged hadron tumour therapy monitoring by means of PET *Nucl. Instrum. Methods* A **525** 284–8

Fiedler F, Crespo P, Sellesk M, Parodi K and Enghardt W 2006 The feasibility of in-beam PET for therapeutic beams of ^{3}He *IEEE Trans. Nucl. Sci.* **53** 2252–9

Hishikawa Y, Kagawa K, Murakami M, Sakai H, Akagi T and Abe M 2002 Usefulness of positron-emission tomographic images after proton therapy *Int. J. Radiat. Oncol. Biol. Phys.* **53** 1388–91

Inaniwa T, Tomitani T, Kohno T and Kanai T 2005 Quantitative comparison of suitability of various beams for range monitoring with induced activity in hadron therapy *Phys. Med. Biol.* **50** 1131–45

Inaniwa T, Kohno T, Tomitani T and Sato S 2008 Monitoring the irradiation field of ^{12}C and ^{16}O SOBP beams using positron emitters produced through projectile fragmentation reactions *Phys. Med. Biol.* **53** 529–42

Iseki Y *et al* 2003 Positron camera for range verification of heavy-ion radiotherapy *Nucl. Instrum. Methods* A **515** 840–9

Jäkel O, Jacob C, Schardt D, Karger C P and Hartmann G H 2001 Relation between carbon ion ranges and x-ray CT numbers *Med. Phys.* **28** 701–3

Krämer M, Jäkel O, Haberer T, Kraft G, Schardt D and Weber U 2000 Treatment planning for heavy-ion radiotherapy: physical beam model and dose optimization *Phys. Med. Biol.* **45** 3299–317

Litzenberg D W, Roberts D A, Lee M Y, Pham K, Vander Molen A M, Ronningen R and Becchetti F D 1999 On-line monitoring of radiotherapy beams: experimental results with proton beams *Med. Phys.* **26** 992–1006

Möckel D, Müller H, Pawelke J, Sommer M, Will E and Enghardt W 2007 Quantification of β^{+} activity generated by hard photons by means of PET *Phys. Med. Biol.* **52** 2515–30

Moehrs S, Defrise M, Belcari N, Del Guerra A, Bartoli A, Fabbri S and Zanetti G 2008 Multi-ray based system matrix generation for 3D PET reconstruction *Phys. Med. Biol.* **53** 6925–45

Nishio T, Ogino T, Nomura K and Uchida H 2006 Dose-volume delivery guided proton therapy using beam on-line PET system *Med. Phys.* **33** 4190–7

Parodi K, Enghardt W and Haberer T 2002 In-beam PET measurements of radioactivity induced by proton beams *Phys. Med. Biol.* **47** 21–36

Parodi K 2004 On the feasibility of dose quantificatin with in-beam PET data in radiotherapy with ^{12}C and proton beams *PhD Thesis, Dresden University of Technology, Germany* (chapter 3)

Parodi K, Pönisch F and Enghardt W 2005 Experimental study on the feasibility of in-beam PET for accurate monitoring of proton therapy *IEEE Trans. Nucl. Sci.* **52** 778–86

Parodi K *et al* 2007 Patient study on in-vivo verification of beam delivery and range using PET/CT imaging after proton therapy *Int. J. Radiat. Oncol. Biol. Phys.* **68** 920–34

Pönisch F, Parodi K, Hasch B G and Enghardt W 2004 The modelling of positron emitter production and PET imaging during carbon ion therapy *Phys. Med. Biol.* **49** 5217–32

Vecchio S *et al* 2007 A PET prototype for 'in-beam' monitoring of proton therapy (NS24-362) *IEEE NSS Conf. Rec. 2007,* 1607–11